Modeling and Simulating Human Fatality due to Quadrotor UAS Impact

Rattanagraikanakorn, B.; Blom, H.A.P.; Sharpanskykh, Alexei; de Wagter, C.; Jiang, C.; Schuurman, M.J.; Gransden, Derek I.; Happee, R.

DOI
10.2514/6.2020-2902

Publication date
2020

Document Version
Final published version

Published in
AIAA AVIATION 2020 FORUM

AIAA AVIATION Forum
June 15-19, 2020, VIRTUAL EVENT
AIAA AVIATION 2020 FORUM

10.2514/6.2020-2902

Modeling and Simulating Human Fatality due to Quadrotor UAS Impact

Borrdephong Rattanagraikanakorn,[1] Henk A.P. Blom,[2] Alexei Sharpanskykh,[3] Christophe De Wagter,[4]
Chengpeng Jiang,[5] Michiel Schuurman,[6]
Delft University of Technology, Kluyverweg 1, 2629 HS Delft, The Netherlands

Derek I. Gransden[7]
Laurentian University, 935 Ramsey Lake Road, Sudbury, Canada

Riender Happee[8]
Delft University of Technology, Mekelweg 2, 2628 CD Delft, The Netherlands

Evaluating safety risk posed to third parties on the ground due to UAS impact requires a model of probability of fatality (PoF) for human. For quadrotor UAS, the existing impact models predict remarkably different PoFs. The most pessimistic is the impact model adopted by Range Commanders Council (RCC) while the Blunt Criterion model is far more optimistic. The ASSURE study has assessed the third set of PoF values through conducting controlled drop tests of a DJI Phantom III on a crash dummy; these results differ again. To investigate these discrepancies, this paper employs a numerical impact analysis of UAS collisions on humans. The current paper is the third in a series of studies. The first study developed a Multi-Body System (MBS) simulation model of a DJI Phantom III impacting the head of a crash dummy; this MBS model has been validated against the experimental drop test results of ASSURE. The second study conducted simulations with the validated MBS model to systematically show the differences in head and neck injuries if the human dummy is replaced by a validated MBS model of a human body. The aim of the current paper is threefold: i) to extend the latter MBS model to assess injury levels for DJI Phantom III impact on thorax and abdomen; ii) to transform the assessed injury levels for head, thorax and abdomen to PoFs; and iii) to compare the MBS obtained PoFs to those from RCC and Blunt Criteria models. The MBS based results show that variations in the scenario of DJI Phantom III impact on the head significantly affect PoF. These variations are not captured by the RCC or BC model, and neither in the ASSURE measurements. Both for head, thorax and abdomen, in case of comparable impact scenarios, the RCC model tends to over-predicts PoF compared to the MBS model, while the BC model tends to under-predict PoF.

[1] Ph.D. Candidate, Section Air Transport and Operation, Faculty of Aerospace Engineering, Delft University of Technology, Kluyverweg 1, 2629 HS Delft, The Netherlands, AIAA member.
[2] Full Professor, Section Air Transport and Operation, Faculty of Aerospace Engineering, Delft University of Technology, Kluyverweg 1, 2629 HS Delft, The Netherlands.
[3] Assistant Professor, Section Air Transport and Operation, Faculty of Aerospace Engineering, Delft University of Technology, Kluyverweg 1, 2629 HS Delft, The Netherlands, non-member.
[4] Researcher, MavLab, Faculty of Aerospace Engineering, Delft University of Technology, Kluyverweg 1, 2629 HS Delft, The Netherlands.
[5] Ph.D. Candidate, Section Air Transport and Operation, Faculty of Aerospace Engineering, Delft University of Technology, Kluyverweg 1, 2629 HS Delft, The Netherlands.
[6] Assistant Professor, Aerospace Structures & Materials Department, Faculty of Aerospace Engineering, Delft University of Technology, Kluyverweg 1, 2629 HS Delft, The Netherlands, AIAA member.
[7] Master Lecturer, Bharti School of Engineering, Laurentian University, 935 Ramsey Lake Road, Sudbury, Canada.
[8] Associate Professor, Cognitive Robotics, Mechanical Engineering, Delft University of Technology, Mekelweg 2, 2628 CD Delft, The Netherlands.

I. Nomenclature

AIS	=	abbreviated injury scale
ATD	=	anthropomorphic test dummy
BC	=	blunt criterion
HIC	=	head injury criterion
POF	=	probability of fatality
RCC	=	Range Commanders Council
TPR	=	third-part risk
UAS	=	unmanned aircraft system
VC	=	viscous criterion

II. Introduction

One of the major challenges of allowing unmanned aircraft system (UAS) operations in rural and urban areas is to predict and subsequently mitigate safety risk posed to third parties on the ground. Models of safety risk posed to third parties on the ground consist of five probabilistic models [1–7]. The first model is for the frequency of a UAS ground crash. The second model is a density map of the rural or urban population. The third model is a shelter protection probability map of the rural and urban area considered. The fourth model is the probability that an unprotected person at a given location is being hit by a UAS crash. The fifth model is for the probability of fatality (PoF) in case of UAS impact of a human on the ground. The literature on the first four of these models shows healthy convergence; but this is not the case for the model of PoF in case of a quadrotor UAS impact on a human.

One of the well-known PoF models of human impact by a UAS has been proposed by Range Commanders Council (RCC) [8]. This model provides PoF curves as a function of the kinetic energy of a UAS at the moment of impact of human head, thorax, and abdomen/limbs respectively. This model is based on the work of Feinstein [9] who assessed these curves on the basis of a large database of collision dynamics and effects of small, rigid, metallic fragments on human. Another impact model of thorax and abdomen injury that is widely used in UAS ground risk analysis [5,10] is the Blunt Criterion (BC) model. BC is an energy-based model developed by Sturdivan [11,12] and has been used by the U.S. Department of Defense to assess vulnerability to blunt weapons, and projectile impacts. Unlike the RCC curves, BC is developed purely for blunt impact force which does not inflict penetration or laceration-type of injury. However, the latter does not explain the large differences between the BC and the RCC models.

To develop a better and applicable approach for UAS impact on the human body based on blunt impact force analysis, the ASSURE Research Group conducted testing and analysis of a DJI Phantom III UAS drop impacts on an anthropomorphic test dummy (ATD) of a human [13,14]. The experiments provide useful insights into impact dynamics between the UAS and the head and neck of the ATD. However, the ASSURE report [13] shows that the RCC model predicts a much higher head injury level than what is measured in the drop tests on the ATD of a human.

To fill the gap between these three different PoF models, the current paper is the third one in a series of studies. In the first study [15], a numerical DJI Phantom III UAS impact model has been developed that is based on a multibody system (MBS) modeling and simulation approach and validated against the ASSURE [14] experimental data. This MBS simulation model allows large variations of UAS impact cases to be evaluated on a validated MBS model of a 50^{th} percentile human body. The second study [16,17] performed a numerical comparison between the Hybrid III crash dummy and the 50^{th} percentile human body model. It was found that the human ATD used (i.e. Hybrid III) has a different biofidelic level when compared to a validated MBS model of a 50^{th} percentile human body. However, the effect of this difference in biofidelity does not explain the much larger differences between ASSURE and the RCC model.

The aim of the current, third study, is to continue the investigation of the differences between the ASSURE data, the RCC curves, and the BC curves for DJI Phantom III impact of human head, thorax, and abdomen. This is realized through three steps. The first step is to extend the MBS model to define and assess relevant injury levels for DJI Phantom III impact on thorax and abdomen of the validated MBS model of a 50^{th} percentile human male body. The second step is to identify valid transformations of the head, thorax and injury levels to PoFs. The third step is a comparison of the MBS obtained PoFs to those from RCC and Blunt Criteria models, and subsequent explanation of how this relates to the ASSURE results.

This paper is organized as follows. Section III reviews the main background. This consists of UAS fatality risk curves from RCC and BC models, as well as the results from our preceding two MBS studies [15–17]. Section IV

presents the extension of the MBS model with injury criteria for thorax and abdomen due to UAS impact, and provides simulations result of DJI Phantom III impacts of the head, thorax, and abdomen as a function of increasing impact energy. Section V addresses the transformation of the MBS measured injury criteria for head, thorax and abdomen to PoF values; this yields PoF curves for DJI Phantom III impacts of head, thorax and abdomen as a function of kinetic energy at impact. Section VI compares the MBS based PoF curves for the head, thorax and abdomen to those of RCC and BC for UAS impact of head, thorax and abdomen. Section VII and VIII present the discussion of the results and the conclusion, respectively.

III. Review of Main Background

A. RCC Fatality Risk Curve

Range Commanders Council proposed a common risk criterion in the Range Commanders Council report (RCC 321-00) where the S-shaped curves were developed to quantify the probability of fatality if a person is impacted in the head, thorax or abdomen by exploded inert debris [8]. These fatality risk curves were based on the work of Feinstein [9] who employed log-normal distributions to relate the probability of fatality to impact which was derived from the study on the effects of the blast, debris, and other factors on human. The log-normal distribution equation for the RCC fatality risk curves is:

$$P_i(Fatality \mid KE < K) = \int_0^K \frac{1}{x\beta_i\sqrt{2\pi}} e^{\frac{-(\ln x - \ln \alpha_i)^2}{2\beta_i^2}} dx \tag{1}$$

where K is the fragment kinetic energy and α_i, β_i are the scale and shape parameters of the log-normal. The parameters for calculating the RCC fatality risk curve accounting for different body parts are listed in Table 1.

Table 1. Log-Normal distribution parameters for different body parts

Body Part	Log-Normal Parameters	
	α	β
Head	55	0.2302
Thorax	44	0.3737
Abdomen	96	0.4335

Using equation (1) and log-normal distribution parameters in Table 1, the PoF curve for the head, thorax, and abdomen can be plotted as shown in Figure 1. The original Feinstein curve is plotted with x-axis in the natural log scale, however, the curve presented is converted into the linear scale for ease of comparison to other models in the later sections of the paper. In Figure 1, the RCC curve shows that fatality due to thorax has a slightly higher probability than the head, and much higher than the abdomen.

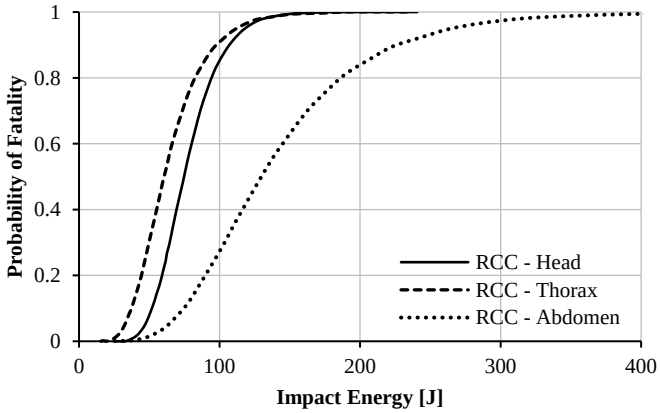

Figure 1. RCC log-normal fatality risk curve for head, thorax and abdomen

The RCC curve shows a steep slope for impact on all body parts. With the RCC curve, the probability of fatality for head and thorax impact reaches 1.0 at approximate 150 J impact energy. With maximum impact energy that DJI Phantom III UAS can achieve (E = 200J), the RCC curve suggests that human fatality is 100% probable if collision on head or thorax occurs. Collision on the abdomen is less severe, with 0.8 probability of fatality at 200 J impact energy. Moreover, impact on the thorax presents a higher fatality risk than the head and abdomen. Explanation of the differences is that the RCC curve is derived from hazardous debris experimentation with the original purpose of determining the fatality risk curve of ground personal due to missile explosions. Such type of small debris explosive injury does not only resolve in blunt force trauma but also penetration or laceration-type injuries.

In addition, the limitations of the RCC standard are rooted in the fundamental assumptions made to generate the curves and the basis for the probability of fatality data. For instance, the RCC curves were developed from Feinstein's work and employed weightings for hypervelocity type collisions where the debris contained a larger number of low mass fragments [13]. Besides, input data that formed Feinstein curves involved largely vertical falling inert debris since it was assumed the breakup or collisions would occur from a high altitude above the personal.

B. Blunt Criterion (BC) Model

Blunt criterion (BC) is proposed by the US Department of Defence and can be used to assess the risk of blunt force trauma from projectiles and blunt weapons [18]. BC was developed based on blunt impact injury data of the thorax [19] which resulted in a five parameters model defined as follow:

$$BC = \ln \frac{E}{W^{1/3} TD} \tag{2}$$

where E in the kinetic energy at impact, W is the mass of an impacted object, T is the thickness of the body wall (in cm), and D is the diameter of impacting object (in cm). It should be noted that W is not the mass of the entire human body, but an effective mass of the body part (head, thorax, or abdomen) which can be calculated using;

$$W = W_{total} \cdot r_{mass} \tag{3}$$

where W_{total} is the total mass of the human body and r_{mass} is the mass body part considered. Typical values of r_{mass} for head, thorax and abdomen are shown in Table 2.

Table 2. Relative body part mass ratio for injury prediction [18]

Body Part	Body part mass ratio, r_{mass}
Head	0.08
Thorax	0.21
Abdomen	0.21

Furthermore, body wall thickness, T, depends mainly on the body part mass and can be calculated by,

$$T = kW^{1/3} \tag{4}$$

where k is equal to 0.711 for thorax and abdomen of a male human. Because BC for head impact was not developed before, the Australian Civil Aviation Safety Authority[20] has developed a BC model for UAS impact of a human head. The approximated body wall thickness T for the male human head is 1.3 cm as reported by the work performed by Raymond [21]. The resulting BC values as a function of increasing Impact kinetic energy are depicted in figure 2 for Head, Thorax and Abdomen.

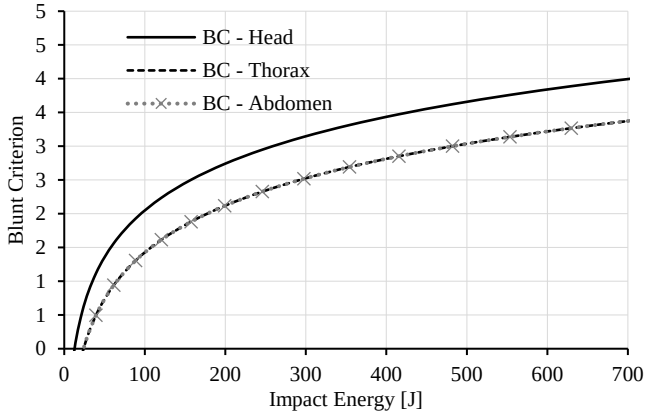

Figure 2. BC results on the head, thorax, and abdomen impact calculated as a function of impact kinetic energy. Note that thorax and abdomen curves overlap because of the identical model parameters for BC model

In order to transform BC values in Figure 2, to PoF values, BC has first to be converted to AIS level using equation (5). Subsequently, the AIS level has to be transformed to PoF values using the curve that is presented in Figure 16. The final results of this PoF transformation for BC model is shown in Figure 3.

$$AIS = 1.33 \cdot BC + 0.6 \tag{5}$$

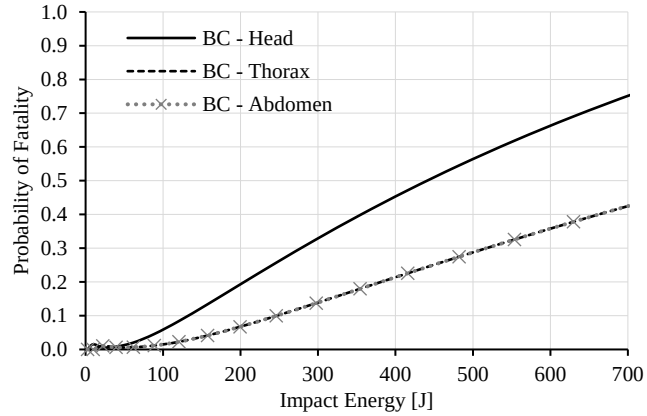

Figure 3. PoF curve from BC model for impact on head, thorax and abdomen as a function of impact kinetic energy. Note that the PoF curves for thorax and abdomen are aligned because the same BC parameters apply for both

Figure 3 shows that the BC model based PoF curve for DJI Phantom III impact of head, thorax and abdomen. It should be noted that the PoF curves for thorax and abdomen are the same because the mass ratio are assumed to be the same. The PoF curve for head is two times steeper than the one for thorax or abdomen. At maximum impact energy of the DJI Phantom III at 200 J, BC predicts 0.2 and 0.08 probability of fatality for head and thorax/abdomen, respectively. Comparison of the BC curves with the RCC curves in Figure 1 shows that the BC curves show a much less steep slope than the RCC curves. The largest difference applies to the PoF curves for head; for the BC model this is much higher than the other two, while the RCC curve is clearly highest for thorax impact instead of head.

C. MBS Modelling and Simulation of DJI Phantom III Impact of Human Head

In automotive and aerospace crashworthiness analysis where an impact is highly dynamic with a range of structures interacting with the human body, multibody system (MBS) modeling is widely adopted [22–25]. These MBS models are only for blunt impact force evaluation, not for the modelling of penetration or laceration injuries. Based on this body of validated knowledge and simulation models, in Rattanagraikanakorn [15] an MBS model of a DJI Phantom III impacting MBS of a human 50th percentile male body has been developed to simulate impact scenarios on the human head. The MBS model and its skeleton model structure is shown in Figure 4. This UAS MBS model consists

of multiple lumped masses that are connected via restraint joints. Ellipsoid surface was modelled to realistically represent external surfaces of the UAS and to be used for contact detection.

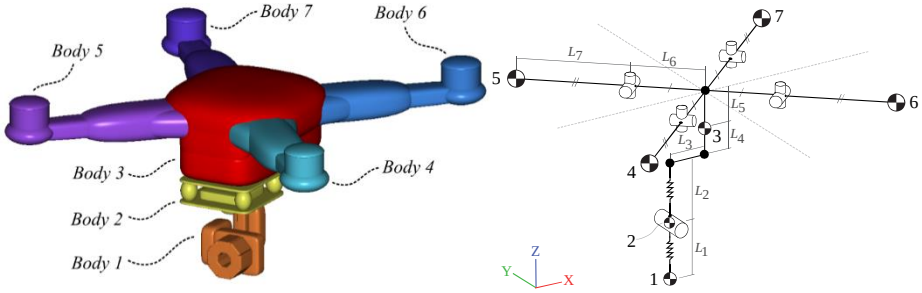

Figure 4. MBS model of the DJI Phantom III UAS (left), and the skeletons of the MBS model (right) [15]

To calibrate the MBS elements of the UAS model in Figure 4, the deformation of the structural components of the real DJI Phantom III system has systematically been measured during deformation experiments. These deformation tests yield curves of joint displacement as a function of restraining force (see Figure 5). Other important parameters such as restraint damping, or inertial properties were also measured experimentally.

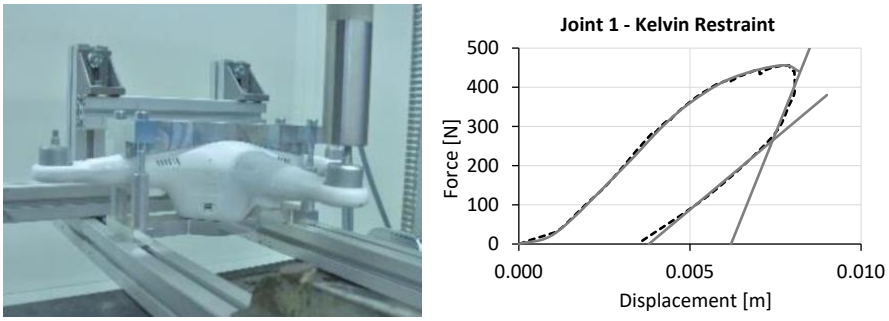

Figure 5. Examples of the compressive static test setup (left) for UAS structural members to determine joint restraint characteristics curves (right) used in model calibration [15]

The calibrated MBS model of DJI Phantom III has subsequently been integrated in MADYMO with a validated MBS model of the Hybrid III ATD. Subsequently, this integrated MBS model has been used to simulate the ASSURE DJI Phantom III UAS impact tests. Comparison of the MBS simulation results to the ASSURE measured data [13] showed that the response of the integrated MBS model was quite similar to the ASSURE measured data; a comparison is shown in Figure 6. The strong similarity in shape and strengths in dynamic responses showed that our MBS model of the DJI Phantom III and its integration within MADYMO was validated, and therefore judged to be ready for follow-on use to other impact studies than the one by ASSURE.

The first follow-on question we have addressed was: what would be the difference in the neck and head injury results when in the ASSURE drop tests the ATD of a human would have been replaced by a true human. Conducting such a test on a real human is not feasible, though such comparison can be done using MBS models of the two situations. Therefore the validated MBS model of DJI Phantom III UAS has been integrated with a validated MBS model of a 50th percentile male human body. The latter was distributed with MADYMO 7.7 (filename: h_occ50fc, version 5.2) and was published by Happee [26,27], and has been validated for blunt impact on head, thorax, abdomen, and limbs [28]. This human body model can be seen in Figure 7. The comparison of these novel integrated MBS model simulations has shown that there is a discrepancy between the Hybrid III ATD and a human body model for head and neck injury [16,17]. Neck loads were found to be different fundamentally between the crash dummy and the human model. The human body sustains larger head injury, but lower neck injury compared to a crash dummy due to the different level of neck compliance between the two. This explains why neck injury assessed and presented in the ASSURE report [13] shows higher PoF from neck injury levels than to the head injury levels. Furthermore, MBS impact analysis on human body shows that the sustained neck injury from DJI Phantom III UAS vertical drop on human head is much lower than head injury.

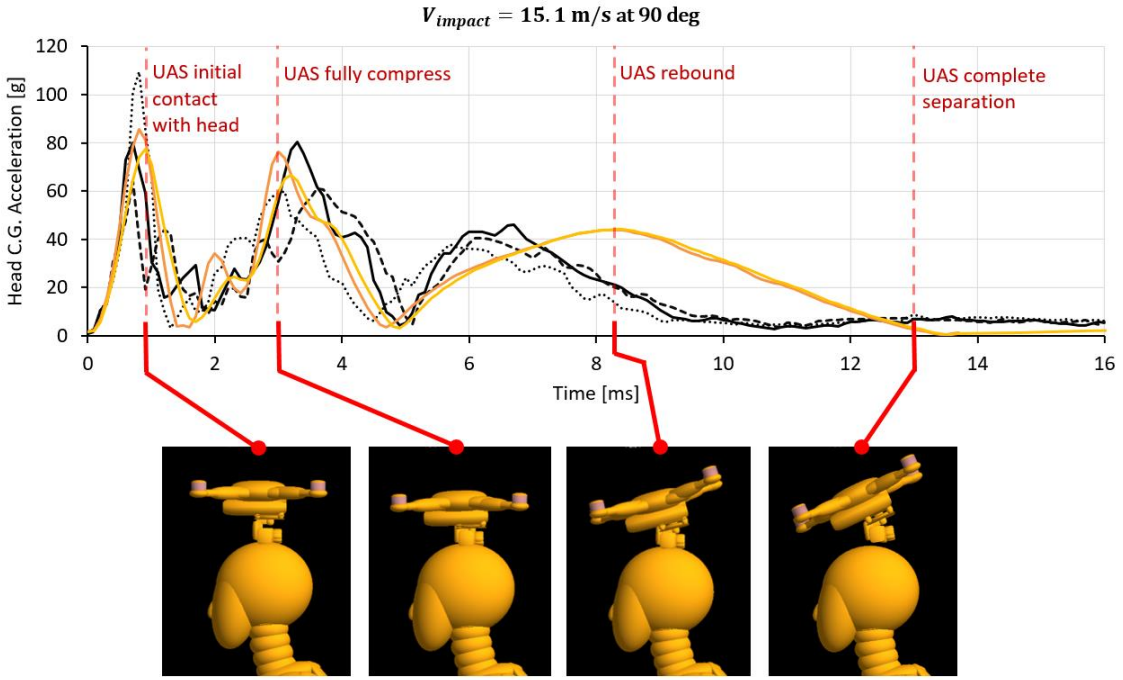

Figure 6. Example of validation results of the MBS model against ASSURE crash dummy impact test data at 15.1 m/s impact velocity and 90° (vertical) impact angle [15]

IV. MBS Simulation-based Assessment of Head, Thorax and Abdomen Injury Criteria

In this section, the MBS model within MADYMO 7.7 of DJI Phantom III impact on 50th percentile human male body of the previous subsection is extended with injury criteria for thorax and abdomen. Subsequently, this extended MBS model is used for the simulation of UAS impact scenarios of head, thorax and abdomen.

A. DJI Phantom III UAS Impact Scenarios

Impacts on head, thorax, and abdomen are evaluated and the simulation setup for each body part is presented in Figure 7. Head impact simulation is performed by varying multiple parameters to cover impact at three different impact conditions, which are frontal, side, and vertical drop impact. This is based on the knowledge that frontal and side-impact cases are the two worst impact cases that result in the highest HIC value based on the previous work [15]. Vertical drop is simulated to show the most optimistic impact case. Similarly, thorax and abdomen impact simulations are set up to evaluate the worst impact case. For both thorax and abdomen impact, frontal impact was setup where UAS fly directly into the body parts at various impact speed.

Head impact injury due to UAS is evaluated based on the setup in Figure 7(a). There are three setup parameters for impact to the head, namely: impact direction (ψ), impact elevation (θ), and impact velocity (V). In this work, three head impact cases are evaluated and the setup parameters are listed Table 3.

Table 3. Setup parameters for head impact cases

Impact Case	ψ [deg]	θ [deg]	V [m/s]
Frontal Impact	0	0	0 - 32 (equivalent to impact energy of 0 – 630 J)
Side Impact	90	0	
Vertical Drop	0	90	

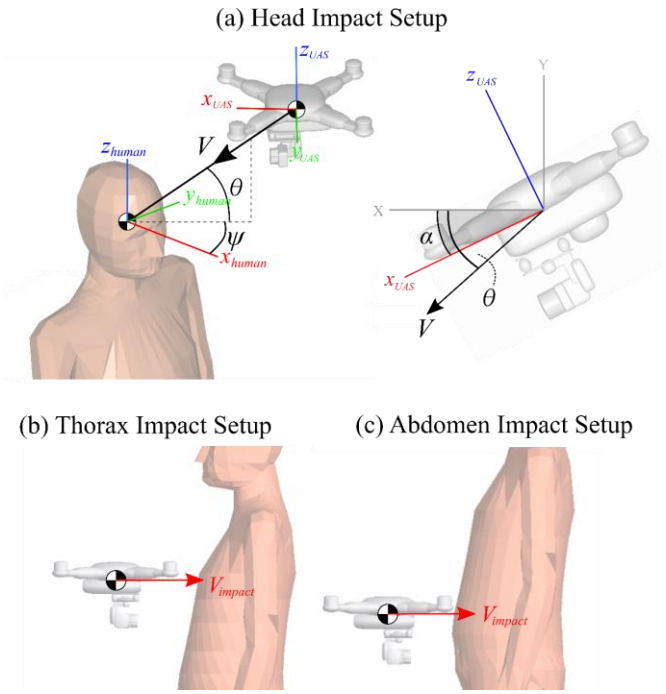

Figure 7. MBS impact model setup in MADYMO

The frontal impact case simulates a UAS flying horizontally into the front of the human head. Side impact also simulates horizontal flight, but onto the side of the human head. Frontal and side-impact cases both have the front fuselage as the first point of contact and are considered as two worst impact cases. A snapshot of the maximum head deflection/deformation for side impact of the head at impact energy of 196 J is pictured in Figure 8.

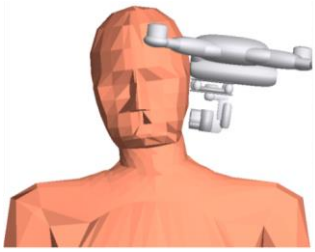

Figure 8. MBS impact simulation results at maximum body part deflection/deformation for side impact on the head at 196 J impact energy

For vertical drop, a UAS is dropped vertically with a fixed angle of attack of 0 degrees. This simulates a straight fall due to the complete power shut-down of a UAS. However, the vertical impact case has the camera gimbal underneath the UAS as the first point of contact. For all three cases, impact velocity (V) is varied from 0 to 32 m/s with a 2 m/s increment. This velocity range is equivalent to an impact energy of 0 to 630 J.

To measure injury level from UAS impact, Head Injury Criterion (*HIC*) is used for head impact, and Viscous Criterion (*VC*) is used for thorax and abdomen impacts. These injury criteria have been used within the MBS simulations. In the next subsections these injury criteria are explained together with the obtained MBS simulation results for the impact scenarios for head, and thorax/abdomen respectively.

B. Head Injury Criteria and MBS Simulation Results

To assess head injury from the UAS impact, the head injury criterion (*HIC*) is used. In particular, HIC_{15} was implemented as it is suitable for short duration impact (The value 15 refers to the 15 *ms* time-period starting from the moment of impact). Functionally, the *HIC* is an integrated value of the head acceleration curve and represents the peak average power delivered to the head [29]. Based on the Federal Motor Vehicle Safety Standards (FMVSS), a HIC_{15} value of 700 is considered to be a minimum safety standard for non-fatal impact [30]. The equations for the *HIC* is:

$$HIC = \left\{ (t_2 - t_1) \left[\frac{1}{t_2 - t_1} \int_{t_1}^{t_2} a(t)dt \right]^{2.5} \right\} \max \tag{6}$$

where $a(t)$ is the head acceleration-time history curve, t_1 is the initial impact time and t_2 is the final impact time.

The simulation results of the head impact on the human body for three impact cases are shown in Figure 9. The simulation results show that HIC_{15} increases with impact energy. Side impact case on the head results in the worst impact case, while frontal impact case also results in severe injury. Vertical drop case, on the other hand, differs significantly from the other curves due to soft impact point.

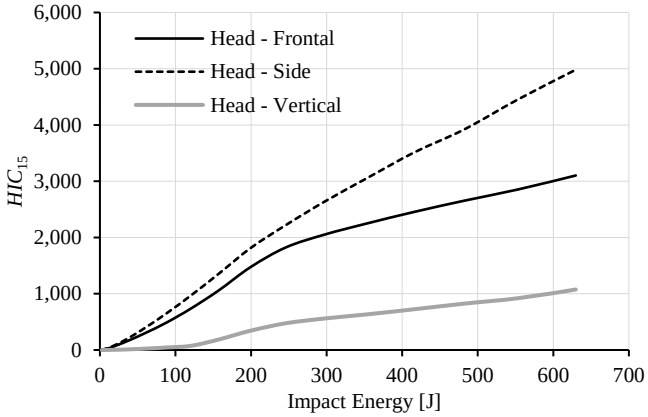

Figure 9. HIC_{15} results for head impact injury from MBS model

C. Thorax and Abdomen Impact Criteria and MBS Simulation Results

Thorax and abdomen present a large portion of the body area and can also be vulnerable to blunt impact force. UAS impact simulation setups on the thorax and abdomen are presented in Figure 7(b) and Figure 7(c), respectively. For thorax and abdomen, there is one setup parameter varied that is impact velocity (V) which is set 0 to 36 m/s with 2 m/s increment. This velocity range is equivalent to impact energy from 0 to 800 J. Only frontal impact cases are evaluated for both thorax and abdomen. This is assumed to be the worst impact case since the velocity vector is normal to the coronal plane of the human body. For impact on the thorax, UAS is placed to collide directly on the sternum. For impact on the abdomen, UAS is placed to collide directly on the mid-abdomen location. These are the common impact locations for thorax and abdomen blunt impact evaluation.

For thorax and abdomen injury evaluation, this paper employs the Viscous Criterion (VC) which is also called the soft tissue criterion. This injury criterion takes into account that soft tissue injury is compression-dependent and rate-dependent [31]. It is a measure of the maximum momentary product of deformation speed and deformation of thorax and abdomen. Hence, for an arbitrary body part B, VC_B satisfies:

$$VC_B(t,r) = \max_{t,r}[V_B(t,r) \times C_B(t,r)] \tag{7}$$

where $V_B(t,r)$ is the deformation speed of body part B at moment t and at location r and $C_B(t,r)$ is the compression in the percentage of the thickness of body part B at moment t and at location r. A VC value of 1.0 m/s is equivalent to 25% of p($AIS \geq 4$); a VC of 1.3 m/s is equivalent to 50% of p($AIS \geq 4$) [18].

For body parts thorax and abdomen, this VC injury criterion is applicable to both frontal impact and side impact. For thorax, compression speed $V_B(t,r)$ and compression $C_B(t,r)$ are measured from the start of impact (i.e. $t = 0$) at sternum ribs r = R1,..,R4 as is illustrated in Figure 10. These are the location for the middle center of the thorax. For abdomen $V_B(t,r)$ and $C_B(t,r)$ are measured from the start of impact on a single point at the mid-abdomen location (or center of the umbilical region).

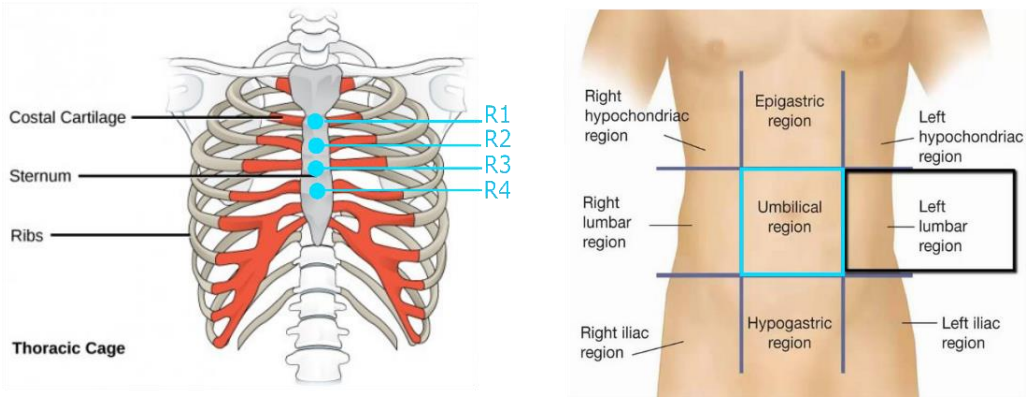

Figure 10. Measuring location for thorax *VC* (left) at sternum rib R1 to R4 and for abdomen *VC* (right) at the center of the umbilical region (or mid-abdomen) [32]

The maximum VC injury criteria given in equation (7) has been implemented in the MADYMO simulation for thorax and abdomen impacts. Figure 11 shows the MBS simulated positions of DJI Phantom and human body at the moment of maximum compression states. The maximum VC simulation results obtained for the thorax and abdomen impact scenarios of a DJI Phantom III UAS are shown in Figure 12 for a range of possible UAS impact velocities.

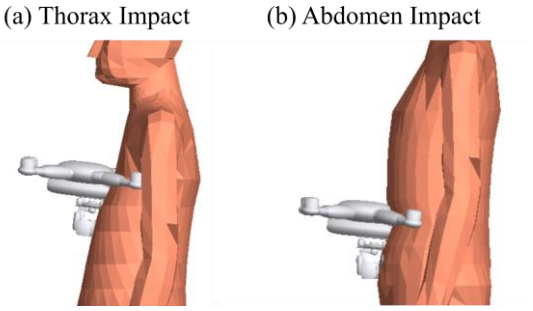

Figure 11. MBS impact simulation results at maximum compression for (a) thorax and (b) abdomen at 196 J impact energy

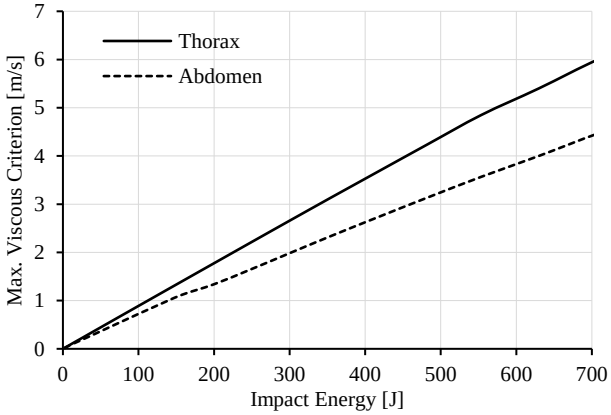

Figure 12. Maximum Viscous Criterion (*VC*) results for thorax and abdomen impact injury from MBS model

The maximum VC curves in Figure 12 show that DJI Phantom III UAS impact on thorax results in a steeper VC curve when compared to the abdomen. Because the injury criteria for head differ from the VC criteria used for thorax and abdomen, a direct comparison of the curves in Figure 12 with those for head in Figure 9 is of no use. Such comparison will be made feasible by identifying appropriate transformations of the curves in figures 9 and 12 to PoF curves. This is addressed in the next section.

V. Mapping Injury Criteria to Probability of Fatality

Injury criteria for head, thorax, and abdomen presents injury severity due to blunt force impact, however, these do not present the probability of fatality. Thus, a mapping of injury criterion to the probability of fatality is needed in order to predict the fatality rate of humans on the ground due to UAS impact.

A. Probability of Fatality Curve for Head impact

For the head injury criterion (*HIC*), a transformational curve from the *HIC* threshold to the percentage of life-threatening injury is proposed by the U.S. ISO Delegation as shown in Figure 13. The curve is derived from the Prasad and Mertz injury risk curve [33]. This percentage of life-threatening injury is equivalent to the probability of fatality. Using this curve, the *HIC* values at different impact energy from Figure 9 for different head impact scenarios are converted to a probability of fatality as shown in Figure 14.

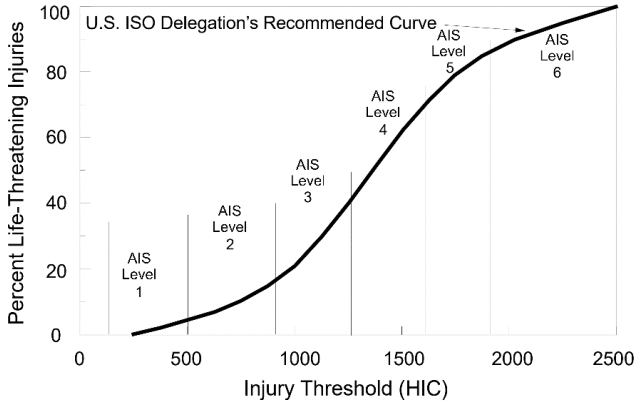

Figure 13. Relationship between head injury criteria and percentage of life-threatening injury recommended by U.S. ISO delegation [34] which is derived from the Prasad and Mertz injury risk curve [33]

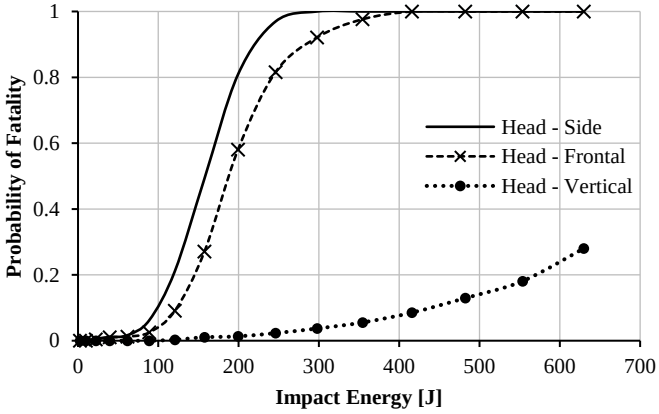

Figure 14. Fatality risk curves of UAS impact on the human head at different impact energy for 50th percentile male and for the side, frontal and vertical drop impact cases

The results from the MBS simulation show that frontal and side impact result in similar PoF, which is much more severe than a vertical drop. Both frontal and side impact curves form an S-curve where PoF gradually increases with impact energy. At impact energy of 200 J which is the estimated maximum impact energy of the DJI Phantom III, PoF of frontal and side are 0.6 and 0.8, respectively. Side impact leads to a more fatal impact when compared to frontal impact because of the way the neck complex plays a role in absorbing impact energy. Impact energy can be absorbed from the head more by neck complex when impact direction falls within the sagittal plane of the human body – this leads to low head acceleration and *HIC* levels.

The vertical drop impact case from the MBS, on the other hand, results in a substantially lower PoF when compared to MBS frontal, and side impacts. The lower curve in Figure 13 shows that at 200 J of impact energy, PoF from the vertical drop impact case is approximately 0.013. Also, with the increasing impact energy, PoF for vertical drop impact

rises with much less slope when compared to other impact cases. This low PoF is a result of having a camera gimbal as the first point of contact. A camera gimbal underneath the UAS acts like a spring-damper system which absorbs impact energy effectively.

The results of the MBS simulation in Figure 14 make very clear that the PoF due to a UAS impact on a human head strongly depends on the specific scenario. The lowest curve in represents the vertical drop on the head scenario that has been considered by the ASSURE drop tests; though now for a 50th percentile male human body instead of the Hybrid III ATD. The two curves with much higher PoF values represent possible case of side or frontal head impact by a flyaway DJI Phantom III UAS. In addition to this, a quadcopter falling trajectory simulation under off-nominal flight conditions performed by Foster and Hartman [35] reveals that quadcopter tends to fall with a high and unpredictable angular rate. This tumbling effect of a quadcopter before colliding into the ground leads to various possible impact attitudes that a quadcopter can impact on a human head. If a DJI Phantom III collides with the main front fuselage, instead of the camera gimbal then the PoF value is expected to be much higher than it is for the vertical drop scenario. The MBS model makes it possible to simulate all possible DJI Phantom III attitudes at moment of head impact.

B. Probability of Fatality Curves for Thorax & Abdomen Impact

The Viscous Criterion (*VC*) for thorax and abdomen injury has no direct transformational curve from *VC* to the probability of fatality. Nevertheless, the transformation of *VC* to the probability of fatality is possible. This is done by, first, converting viscous criterion to *AIS* scale using a conversion curve shown in Figure 15. The curve is proposed by Sturdivan [18] who performed an analysis of VC for thorax and abdomen. This curve is based on a blunt impact experiment on cadavers performed by Canavaugh [36] and Viano [37].

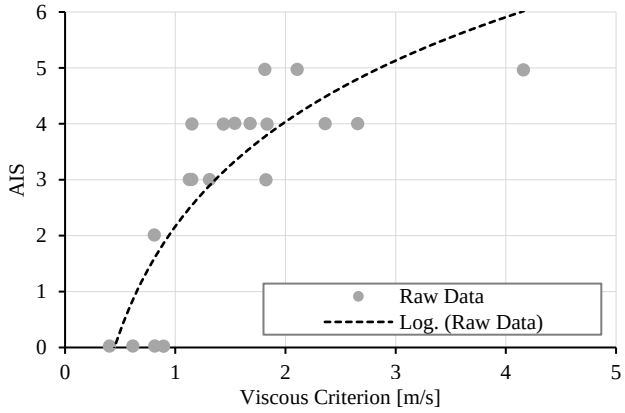

Figure 15. Relationship between Viscous Criterion and AIS[18] **from thoracic and abdominal blunt impact, derived from cadaver impact data performed by Canavaugh [36] and Viano [37]**

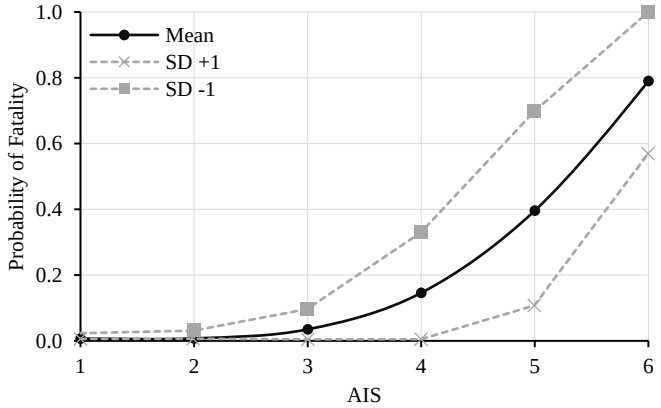

Figure 16. Transformation curve of single injury AIS scale to the probability of fatality presented in the AIS 2005 revision document [38]

The next step is to transform the *AIS* level that is obtained from *VC-AIS* conversion into a PoF using the *AIS* to fatality rate curve presented in Figure 16. This curve is a transformational curve of single injury that is derived from a collection of real-world trauma injury data presented in the AIS 2005 revision document [38]. Application of these two transformations to the MBS based BC curves in Figure 11 yields the MBS based PoF curves for thorax and abdomen in Figure 17. The MBS simulation based PoF curves in Figure 17 show that the impact on thorax is less fatal than the frontal or side impacts on the head as is shown in Figure 14. At impact energy of 200 J, the MBS model based PoF value for frontal impact on the head is approximately 8 times higher than the PoF value for impact on thorax.

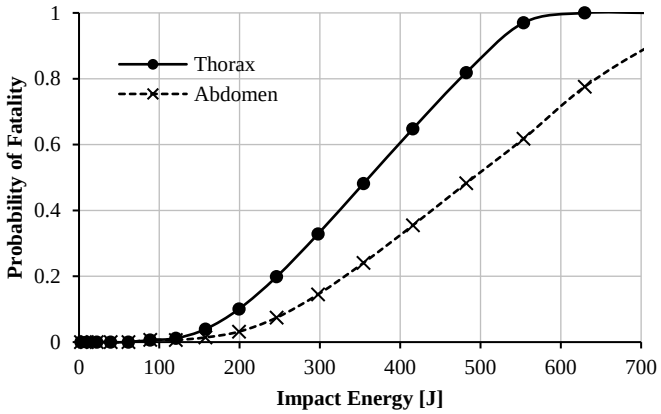

Figure 17. PoF curves of UAS impact on thorax and abdomen at different impact energy for 50th percentile male

VI. Comparison of Fatality Curves from Different Models

This section compares the PoF curves in Figure 14 and Figure 17 with those of the RCC and BC models. This is done for head, thorax and abdomen in subsections A, B, and C respectively.

A. Comparison of PoF of Head Impact

In Figure 18, the PoF curves from MBS head impact simulation from Figure 14 are compared against the RCC and BC curves. Figure 18 shows that both the MBS based PoF curves for frontal and side impact of head and the RCC based PoF curves are S-shaped, though their 10%, 50% and 90% points differ significantly. When the RCC curve has reached the 90% point then the MBS based curves for side and frontal head impacts are around 10% only. The BC curve is not an S-shaped curve, instead it increases more linear with impact energy. As has been explained in subsection V.A the MBS based PoF curve for vertical drop shows the lowest fatality risk.

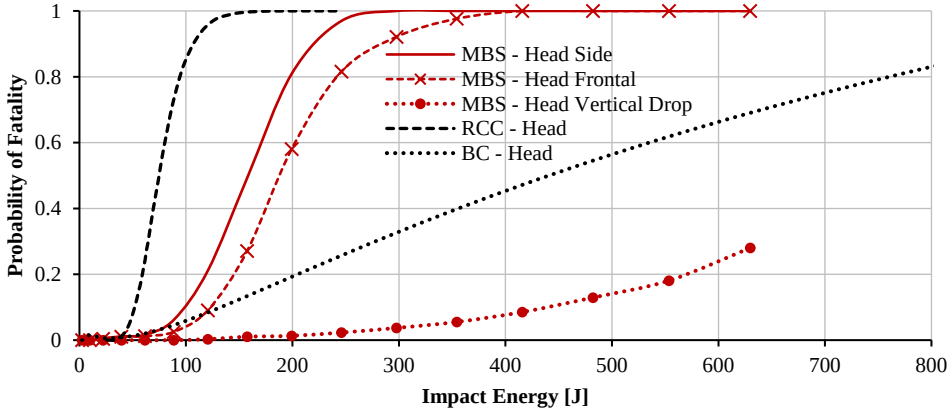

Figure 18. Comparison of PoF curves for head impact between MBS (frontal, side and vertical drop cases), RCC, and BC

From the MBS model results, it becomes clear that PoF of UAS impact of head can have a large difference between upper and lower bound curves. From the three scenarios considered, in this paper, head frontal impact represents the upper bound of the possible fatality risk while head vertical drop impact represents the lower bound. This variation is

not captured by the RCC model, and neither by the BC model. From the perspective of the vertical drop on a human head, Figure 18 shows that both the RCC curve and the BC curve overestimate the PoF. From the perspective of a side or frontal impact the RCC curve again overestimates the PoF, while the BC curve underestimates the PoF. Therefore, the main finding for UAS impact of human head is that where the RCC and BC curves for PoF do not represent differences in impact geometry, the PoF curves obtained through MBS simulation show significant differences for the three different head impact scenarios for frontal, side, and vertical drop respectively.

B. Comparison of PoF of Thorax Impact

The PoF curves obtained for impact on thorax from MBS, RCC, and BC models, from Figures 17, 1 and 3 respectively, are collected in Figure 19. Similar to side or frontal head impact, the PoF values of the RCC curve are much higher than the PoF values for the MBS model; though now the difference is even much larger. Both MBS and RCC curves for impact on thorax are S-shaped; though the 10%, 50% and 90% points of the MBS curve are at much higher kinetic energy levels than the 10%, 50% and 90% of the RCC curve. Again, the BC curve increases more linear with impact energy and has beyond the 10% point a less steep slope than the MBS curve has.

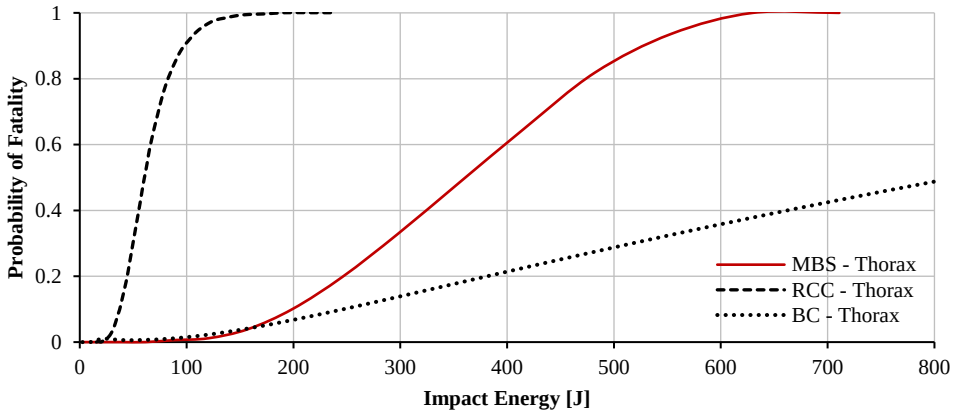

Figure 19. Comparison of PoF curves for thorax impact between MBS, RCC, and BC models

MBS PoF curve increases steadily between impact energy from approximately 250 J to 450 J. Due to its steep slope, this range of steady increase is much smaller for the RCC curve and have energy values between 40 J – 70 J. At maximum impact energy for the DJI Phantom III at 200 J, PoF predicted by the RCC model is 1.0, meaning that fatality from impact on thorax is certain. This is different for the MBS and BC models where PoF at 200 J impact energy is 0.1 and 0.07, respectively. Based on this difference at 200 J impact energy, RCC predicts PoF 10 times higher compared to MBS models.

C. Comparison of PoF of Abdomen Impact

The results of PoF curves of impact on the abdomen from MBS, RCC, and BC models, from Figures 17, 1 and 3 respectively, are collected in Figure 20. For impact on the abdomen, the RCC and MBS models, again, form an S-curve pattern; again the 10%, 50% and 90% points are much lower for RCC curve than for the MBS based curve. Similar as for thorax, the BC curve increase more linear with impact energy, and is much lower than the MS curve for probabilities above 10%.

PoF at 100 J impact energy by DJI Phantom III is 0.27 for the RCC model, but close to 0 for the MBS and BC models. This means that the MBS and BC models predict that UAS impact on the abdomen will not likely result in fatality at 100 J impact energy. At 200 J impact energy which is the maximum energy for DJI Phantom III, PoF predict by the MBS model is 0.05. This is lower than the BC model which predicts 0.07 PoF at the same impact energy. The MBS PoF curve is below the BC curve from 0 J to approximately 295 J. Then, the MBS PoF curve rises and crosses above the BC model after 295 J with substantially higher slope.

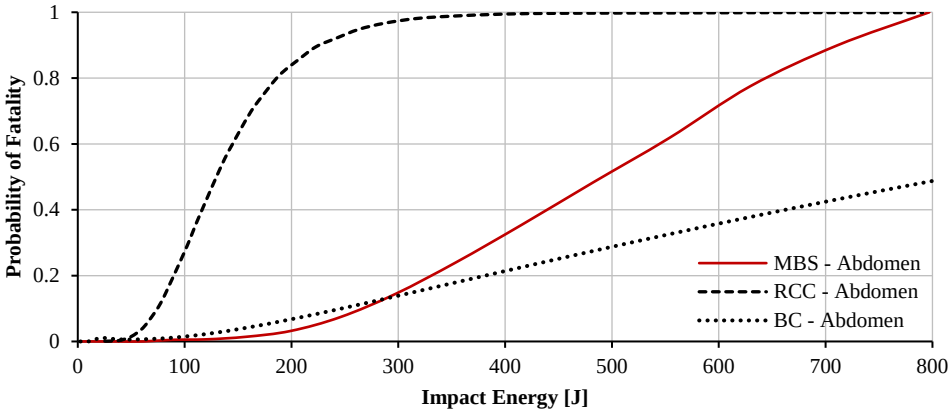

Figure 20. Comparison of PoF curves for abdomen impact between MBS, RCC, and BC models

VII. Discussion of Results

Modelling PoF due to UAS impact is crucial in the analysis of UAS ground risk. Simulation of a validated MBS model of DJI Phantom III UAS impact on a validated MBS model of 50th percentile male human body offers the capability to simulate the impact on different parts of the human body. MBS simulations of DJI Phantom III impact on head, thorax and abdomen shows that the riskiest impact case on the head presents much higher fatality risks when compared to the riskiest impact case on thorax or abdomen. This trend is the same for the BC model but differs for the RCC model. In the RCC model, impact injury on thorax presents a higher PoF than impact on abdomen, though also higher than side or frontal impact on the head. Explanation of the differences is that the RCC curve is derived from hazardous debris experimentation with the original purpose of determining the fatality risk curve of ground personal due to missile explosions. Such type of small debris explosive injury does not only result in blunt force trauma but also penetration or laceration-type injuries. On the other hand, the MBS impact model and BC model are created or derived specifically for blunt impact injury where soft tissue penetration is not involved. For instance, the BC model was developed based on impact tests on cadavers and animals where the diameter of the impactor is much larger than small debris explosion as mentioned in Feinstein's work. Similarly, the MBS impact model of a DJI Phantom III UAS developed and validated against real-world impact tests on the Hybrid III crash dummy where only blunt force injury is evaluated.

RCC model tends to predict a high probability of fatality at low impact energy. For example, the probability of the fatality of head impact is at 0.8 at 100 Joules impact energy. Given that the DJI Phantom III maximum kinetic energy is approximately 200 Joules, this means that fatality is very likely even if the UAS impact at half of its kinetic energy. RCC model predicts too high PoF values. On the other end of the spectrum, BC predicts the probability of fatality of head impact 0.2 at 200 Joules of impact energy. When compared to the MBS model, above 10% values, BC predicts too low PoF values. The limitations of the RCC standard are rooted in the fundamental assumptions made to generate the curves and the basis for the probability of fatality data. For instance, the RCC curves were developed from Feinstein's work and employed weightings for hypervelocity type collisions where the debris contained a larger number of low mass fragments [13]. Also, input data that formed Feinstein curves involved largely vertical falling inert debris since it was assumed the breakup or collisions would occur from a high altitude above the personal. Therefore, the analysis shows that the RCC is not a suitable curve to be used for UAS blunt impact on human body.

Furthermore, what the MBS model show is that the probability of fatality depends significantly on impact attitude and point of contact of the UAS as shown in Figure 18. Side impact results in the steepest fatality curve when compared to frontal impact or vertical drop because the human neck complex can absorb less impact energy in a lateral direction. In the vertical drop case, the fatality curve drops significantly even lower than thorax and abdomen impact cases. This is due to the point of contact for the vertical drop is the camera gimbal system which acts like a spring-damper that absorbs a significant amount of impact energy. This illustrates that single PoF curve models such as the RCC or BC models, do not capture this effect due to the variation of impact attitude of a DJI Phantom III UAS.

VIII. Conclusions

Risk analysis of UAS ground impact on humans is important to the future developments of UAS operations. An important step to take is to understand fatality of UAS impact on human on the ground. In this paper, a multi-body system impact model of the DJI Phantom III UAS is presented and compared against RCC impact model and Blunt Criterion model. The comparison is done for impacts on the head, thorax, and abdomen of a 50th percentile male human. The results show significant differences between the three models in terms of the probability of fatality. RCC model predicts a very high probability of fatality at very low impact energy when compared against MBS or BC model. On the optimistic end of the spectrum, the BC model predicts the lowest probability of fatality when compared to other models. The MBS model shows large variations in PoF for impact on the head. This large variation comes from different impact attitudes. The by far worst impact case from the MBS simulations yields a PoF curve that means more safety than the corresponding RCC curve. The by far the best impact case from the MBS was the DJI Phantom III vertical drop scenario that was also measured by ASSURE.

Furthermore, the MBS and BC model predicts higher fatality for head impact compared to thorax and abdomen. RCC curves, however, predict higher fatality for thorax than the head and abdomen. The differences stem from the fact that the RCC model was derived based on injury or fatality due to small debris explosion, which also involves penetration or laceration type injuries. MBS and BC model, in contrast, were developed purely on blunt force impact.

Taking all results together, it is concluded that thanks to the MBS modelling and simulation of DJI Phantom III UAS impact on human head, thorax and abdomen, it is now possible to understand why there are such differences between the RCC model, the BC model and the ASSURE measurements.

As follow on research, the aim is to use the validated MBS model simulation as a replacement of the RCC and BC models that have so far been used in other works [1–7] on assessing third party risk that is posed by UAS operations to persons on the ground. As has been explained in the introduction, this asks for integration of MBS model simulation with four other models, i.e.: Frequency of a UAS ground crash; Density map of rural or urban population; Shelter protection map; and Model for the probability that an unprotected person on the ground is impacted by the crashing UAS. This MBS approach also allows to consider other variations, such as effect of human body sizes that are available within MADYMO, namely, 5th percentile female, 50th percentile male, and 95th percentile male.

References

[1] Dalamagkidis, K., Valavanis, K., and Piegl, L., "On Integrating Unmanned Aircraft Systems into the National Airspace System," Springer Netherlands, 2012, doi: 10.1007/978-94-007-2479-2.

[2] Melnyk, R., Schrage, D., Volovoi, V., and Jimenez, H., "A third-party casualty risk model for unmanned aircraft system operations," *Reliability Engineering and System Safety*, vol. 124, 2014, pp. 105–116, doi: 10.1016/j.ress.2013.11.016, URL: http://dx.doi.org/10.1016/j.ress.2013.11.016.

[3] Ancel, E., Capristan, F. M., Foster, J. V., and Condotta, R. C., "Real-time Risk Assessment Framework for Unmanned Aircraft System (UAS) Traffic Management (UTM)," *17th AIAA Aviation Technology, Integration, and Operations Conference,Denver, Colarado*, 2017, pp. 1–17, doi: 10.2514/6.2017-3273, URL: https://arc.aiaa.org/doi/10.2514/6.2017-3273.

[4] Bertrand, S., Raballand, N., Viguier, F., and Muller, F., "Ground risk assessment for long-range inspection missions of railways by UAVs," *2017 International Conference on Unmanned Aircraft Systems, ICUAS 2017*, 2017, pp. 1343–1351, doi: 10.1109/ICUAS.2017.7991331.

[5] la Cour-Harbo, A., "Quantifying Risk of Ground Impact Fatalities for Small Unmanned Aircraft," *Journal of Intelligent and Robotic Systems: Theory and Applications*, vol. 93, 2019, pp. 367–384, doi: 10.1007/s10846-018-0853-1.

[6] Rudnick-Cohen, E., Herrmann, J. W., and Azarm, S., "Modeling Unmanned Aerial System (UAS) Risks via Monte Carlo Simulation," *2019 International Conference on Unmanned Aircraft Systems (ICUAS)*, 2019, pp. 1296–1305, doi: 10.1109/icuas.2019.8798313.

[7] Primatesta, S., Rizzo, A., and la Cour-Harbo, A., "Ground Risk Map for Unmanned Aircraft in Urban Environments," *Journal of Intelligent and Robotic Systems: Theory and Applications*, 2019, doi: 10.1007/s10846-019-01015-z.

[8] RCC, “Common risk criteria for National test ranges; Inert debris, Supplement to Standard 321-00,” 2000.

[9] Feinstein, D., Haugel, W., Kardatzke, M., and Weinstock, A., “Personnel Casualty Study. Tech. Rep. Project No. J 6067,” 1968.

[10] Magister, T., “The small unmanned aircraft blunt criterion based injury potential estimation,” *Safety Science*, vol. 48, 2010, pp. 1313–1320, doi: 10.1016/j.ssci.2010.04.012, URL: http://dx.doi.org/10.1016/j.ssci.2010.04.012.

[11] Sturdivan, L. M., “Modeling in Blunt Trauma Research,” *Proceedings of the Second Annual Soft Body Armor Symposium*, Miami, Beach Florida: Washington DC: Law Enforcement Assistance Agency, U.S. Department of Justice, 1976.

[12] Sturdivan, L. M., “Non-Lethal Weapons Assessment: Deterrence and Injury - Final Report. Contract M67854-99-M-1062,” Quantico, VA: 2000.

[13] Arterburn, D., Ewing, M., Prabhu, R., Zhu, F., and Francis, D., “FAA UAS Center of Excellence Task A4 : UAS Ground Collision Severity Evaluation,” Huntsville: 2017, URL: http://www.assureuas.org/projects/deliverables/a4/ASSURE_A4_Final_Report_UAS_Ground_Collision_Severity_Evaluation.pdf.

[14] Alliance for System Safety of UAS through Research Excellence, “ASSURE UAS Ground Collision Severity Evaluation Final Report” URL http://www.assureuas.org/projects/deliverables/sUASGroundCollisionReport.php.

[15] Rattanagraikanakorn, B., Gransden, D. I., Schuurman, M., De Wagter, C., Happee, R., Sharpanskykh, A., and Blom, H. A. P., “Multibody system modelling of unmanned aircraft system collisions with the human head,” *International Journal of Crashworthiness*, vol. 0, 2019, pp. 1–19, doi: 10.1080/13588265.2019.1633818, URL: https://doi.org/10.1080/13588265.2019.1633818.

[16] Rattanagraikanakorn, B., Schuurman, M. J., Gransden, D. I., Happee, R., Wagter, C. De, Sharpanskykh, A., and Blom, H. A., “Modelling Head Injury due to Unmanned Aircraft Systems Collision: Crash Dummy vs Human Body,” *AIAA Aviation 2019 Forum*, Dallas, Texas: 2019, doi: 10.2514/6.2019-2835, URL: https://arc.aiaa.org/doi/abs/10.2514/6.2019-2835.

[17] Rattanagraikanakorn, B., Schuurman, M., Gransden, D. I., Happee, R., Wagter, C. De, Sharpanskykh, A., and Blom, H. A. P., “Modelling Head Injury due to Unmanned Aircraft Systems Collision: Crash Dummy vs Human Body,” *International Journal of Crashworthiness (Submitted for publication)*, 2020.

[18] Sturdivan, L. M., Viano, D. C., and Champion, H. R., “Analysis of Injury Criteria to Assess Chest and Abdominal Injury Risks in Blunt and Ballistic Impacts,” *Journal of Trauma - Injury, Infection and Critical Care*, vol. 56, 2004, pp. 651–663, doi: 10.1097/01.TA.0000074108.36517.D4.

[19] Clare, V., and Sturdivan, L. M., “Blunt Trauma Data Correlation,” 1975.

[20] Civil Aviation Safety/Monash University, “Human Injury Model for Small Unmanned Aircraft Impacts,” 2013.

[21] Raymond, D., Van Ee, C., and Bir, C., “Tolerance of the skull to blunt ballistic temporo-parietal impact,” *Journal of Biomechanics*, vol. 42, 2009, pp. 2479–2485.

[22] Vadlamudi, S., Blundell, M., and Zhang, Y., “A multi-body systems approach to simulate helicopter occupant protection systems,” *International Journal of Crashworthiness*, vol. 16, 2011, pp. 207–218, doi: 10.1080/13588265.2011.554203.

[23] Jenefeldt, F., and Thomson, R., “A methodology to assess frontal stiffness to improve crash compatibility,” *International Journal of Crashworthiness*, vol. 9, 2004, pp. 475–482, doi: 10.1533/ijcr.2004.0303.

[24] Mukherjee, S., Chawla, A., Nayak, A., and Mohan, D., “Rollover crashworthiness of a rural transport vehicle using MADYMO,” *International Journal of Crashworthiness*, vol. 11, 2006, pp. 495–503, doi: 10.1533/ijcr.2005.0121.

[25] Ambrósio, J., and Dias, J., “A road vehicle multibody model for crash simulation based on the plastic hinges approach to structural deformations,” *International Journal of Crashworthiness*, vol. 12, 2007, pp. 77–92, doi:

10.1533/ijcr.2006.0171.

[26] Happee, R., Hoofman, M., Van Den Kroonenberg, A. J., Morsink, P., and Wismans, J., "A Mathematical Human Body Model for Frontal and Rearward Seated Automotive Impact Loading," *SAE Technical paper*, 1998, doi: 10.4271/983150.

[27] Happee, R., and Ridella, S., "Mathematical human body models representing a mid size male and a small female for frontal, lateral and rearward impact loading," *IRCOBI Conference Proceedings*, 2000, pp. 1–18, doi: 10.1378/chest.120.6_suppl.464S.

[28] TASS International, "Human Body Models Manual Version 7.7," 2017.

[29] Hutchinson, J., Kaiser, M. J., and Lankarani, M., "The Head Injury Criterion (HIC) functional," *Journal of Applied Mathematics and Computation*, 1998.

[30] Eppinger, R., Sun, E., Bandak, F., Haffner, M., Khaewpong, N., Maltese, M., Kuppa, S., Nguyen, T., Takhounts, E., Tannous, R., Zhang, A., and Saul, R., "Development of Improved Injury Criteria for the Assessment of Advanced Automotive Restraint Systems - II By," 1999, URL: https://www.nhtsa.gov/sites/nhtsa.dot.gov/files/rev_criteria.pdf.

[31] Lau, I. V., and Viano, D. C., "The viscous criterion - Bases and applications of an injury severity index for soft tissues," *SAE Technical Papers*, vol. 95, 1986, pp. 672–691, doi: 10.4271/861882.

[32] Schmitt, K.-U., Niederer, P. F., Cronin, D. S., Morrison III, B., Muser, M. H., and Walz, F., "Trauma Biomechanics," 2019, doi: 10.1007/978-3-030-11659-0.

[33] Prasad, P., and Mertz, H. J., "The Position of the United States Delegation to the ISO Working Group 6 on the Use of HIC in the Automotive Environment," *SAE Technical Papers*, 1985, doi: 10.4271/851246.

[34] Tyrell, D. C., Severson, K. J., and Marquis, B. P., "Analysis of occupant protection strategies in train collisions," *American Society of Mechanical Engineers, Applied Mechanics Division, AMD*, vol. 210, 1995, pp. 539–557.

[35] Foster, J. V., and Hartman, D., "High-Fidelity Multi-Rotor Unmanned Aircraft System (UAS) Simulation Development for Trajectory Prediction Under Off-Nominal Flight Dynamics," *17th AIAA Aviation Technology, Integration, and Operations Conference*, 2017, pp. 1–19, doi: 10.2514/6.2017-3271, URL: https://arc.aiaa.org/doi/10.2514/6.2017-3271.

[36] Cavanaugh, J. M., Walilko, T. J., Malhotra, A., Zhu, Y., and King, A. I., "Biomechanical response and injury tolerance of the pelvis in twelve sled side impacts," *SAE Technical Papers*, vol. 99, 1990, pp. 1678–1693, doi: 10.4271/902305.

[37] Viano, D. C., Lau, I. V., Asbury, C., King, A. I., and Begeman, P., "Biomechanics of the human chest, abdomen, and pelvis in lateral impact," *Accident Analysis and Prevention*, vol. 21, 1989, pp. 553–574, doi: 10.1016/0001-4575(89)90070-5.

[38] Gennarelli, T. A., and Wodzin, E., "AIS 2005: A contemporary injury scale," *Injury*, vol. 37, 2006, pp. 1083–1091, doi: 10.1016/j.injury.2006.07.009.